

Simulation of Near-Source Ground Motions with Dynamic Failure
Brad T. Aagaard, John F. Hall, and Thomas H. Heaton
May 2000

ABSTRACT

We simulate long-period near-source ground motions due to hypothetical events on a strike-slip fault (Mw 6.9) and a buried thrust fault (Mw 7.0). We include the dynamics of the rupture process using a model of sliding friction. The directivity of the rupture creates large displacement and velocity pulses in the ground motions in the forward direction. For the strike-slip fault the peak values occur near the tip of the fault, while for the buried thrust fault the peak values occur up-dip from the top of the fault. The acceleration response spectra in the 2.0 sec to 3.0 sec range exceed 1.0 g near the strike-slip fault in the forward direction, and 0.5 g up-dip from the top of the thrust fault. These results quantify the threat posed to long-period structures near faults.

INTRODUCTION

Several recent earthquakes, such as Northridge and Kobe, have demonstrated the importance of understanding the relationship between how faults rupture and the resulting ground motions. These moderate earthquakes occurred near large centers of population and caused substantial damage. We focus on improving our understanding of near-source ground motions by including the dynamics of the rupture process in the simulations through a model of sliding friction on the fault surface. These ruptures with dynamic failure produce complex behavior that is not easily incorporated into prescribed ruptures with specified source parameters (Aagaard 1999). While we have examined many hypothetical scenarios on a strike-slip fault and a thrust fault (Aagaard 1999), here, we present only one scenario for each fault in order to illustrate many of the general features present in the simulations.

METHODOLOGY

We solve for the ground motion time histories using the three-dimensional, dynamic, elasticity equation. Using the finite-element method (the details may be found in Rao (1999) or other finite-element texts), we turn the elasticity equation into a matrix equation and compute the ground motions for periods greater than 2.0 sec. Aagaard (1999) provides a detailed discussion of the methodology. The highly variable node spacing and minimal storage requirements of the tetrahedral finite-element with four nodes allow efficient modeling of domains with heterogeneous material properties (Bao et al. 1998). We numerically integrate the matrix differential equation using the central difference scheme, because it requires minimal computation effort and is well-suited for parallel processing. Simulations that involve millions of degrees of freedom require gigabytes of memory and billions of floating point operations. Parallel computing provides a suitable environment for solving such problems by distributing the memory and computation among many processors.

We build the fault plane into the geometry of the finite-element model. Each fault node has six translational degrees of freedom that are split such that each side of the fault has the usual three translational degrees of freedom. By transforming the degrees of freedom on the fault plane to relative and average degrees of freedom, we gain control of the friction stress on the fault. We do not need to know the initial stresses

throughout the domain to model the wave propagation or to simulate the dynamic failure on the fault; we only need to know the initial stresses acting on the fault surface. We generate these stresses from a uniform strain field.

We choose to use a simple, *ad hoc* friction model that produces realistic rupture behavior and captures the general features of more complicated models. The coefficient of friction in this slip-weakening friction model decreases linearly over some characteristic slip distance, D_o , as shown in figure 1. We use a characteristic slip distance of 0.3 m. We compute the friction stress from the product of the normal stress on the fault and the coefficient of friction, where the normal stress equals the overburden pressure. In order to create relatively uniform distributions of slip with depth, the coefficient of friction decreases as the ratio of the square root of the shear modulus to the depth. The values of u_{\max} and u_{\min} vary from 0.16 and 0.023 at the ground surface to 0.034 and 0.0048 at a depth of 15 km.

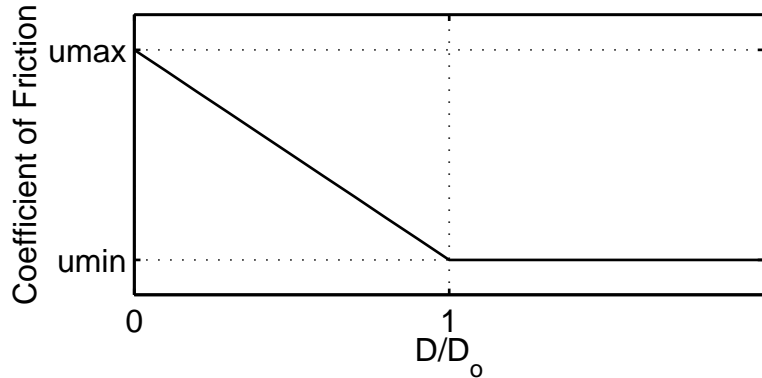


Figure 1: Slip-weakening friction model.

RESULTS

We study the characteristics of the rupture behavior and the resulting ground motions on a strike-slip fault and a shallow dipping thrust fault in a layered half-space. We also compute response spectra at selected locations.

Strike-Slip Fault

The geometry of the strike-slip fault roughly matches the combined fault segments that ruptured in the June 1992 Landers event. We enclose the 60 km long and 15 km wide fault in a domain 100 km long, 40 km wide, and 32 km deep as shown in figure 2. Figure 3 shows the mass density, shear wave speed, and dilatational wave speed as a function of depth in the layered half-space. The finite-element model contains 6.3 million degrees of freedom and 10 million elements.

We derive the initial shear tractions on the fault surface from application of uniform shear strains. We initiate the rupture using a circular asperity located 14 km from the end of the fault (labeled H in figure 2), where the shear stresses inside the asperity exceed the failure stresses by 2%. The rupture propagates across the fault at a rupture speed between 75% and 90% of the local shear wave speed in the direction of slip. We attribute the variation in the rupture speed to an increase in the maximum slip rates as the rupture approaches the ground surface and encounters a reduction in stiffness. Figure 4 shows the distribution of the final slip. The average slip of 1.9 m corresponds

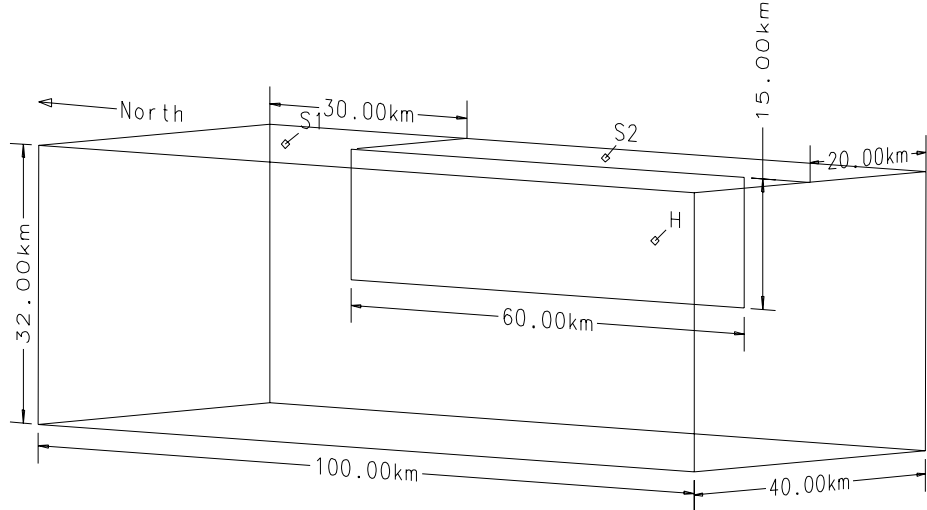


Figure 2: Domain geometry for the strike-slip fault.

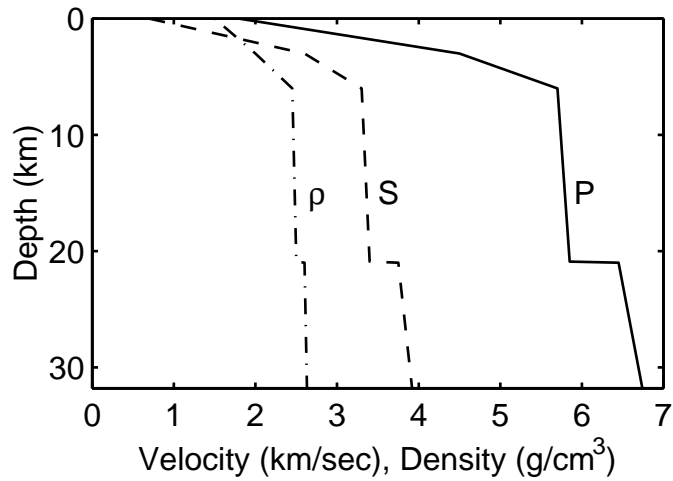


Figure 3: Mass density (ρ), shear wave speed (S), and dilatational wave speed (P) as a function of depth in the layered half-space.

to a moment magnitude of 6.9. The region where the final slip exceeds 3.0 m coincides with the locations that are subjected to a second slip event associated with the reflection of the rupture off the ground surface. This appears to distort the final slip from a more uniform distribution.

The distributions of the maximum horizontal displacements and velocities in figure 5 clearly show the effect of the directivity of the rupture. Both the maximum displacements and velocities increase along the strike of the fault away from the epicenter until the end of the fault where they begin to decay. On the ground surface the maximum displacements exceed 1.0 m over an area of 1200 square kilometers with a peak value of 3.0 m, and the maximum velocities exceed 1.0 m/sec over an area of 550 square kilometers with a peak value of 3.5 m/sec. The maximum displacements exhibit a more gradual decay away from the fault than the velocities which display a teardrop shape.

We now examine acceleration response spectra at sites S1 and S2 (see figure 2 for locations of the sites). We rotate the waveforms into the direction with the maximum

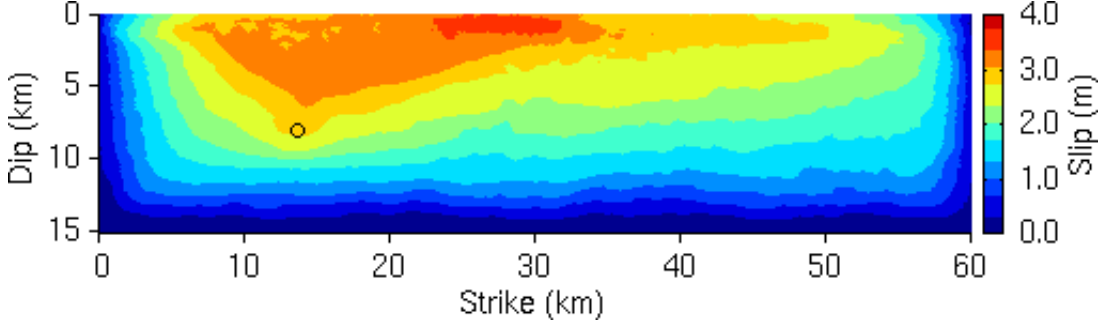


Figure 4: Distribution of final slip at each point on the strike-slip fault. The black circle indicates the hypocenter.

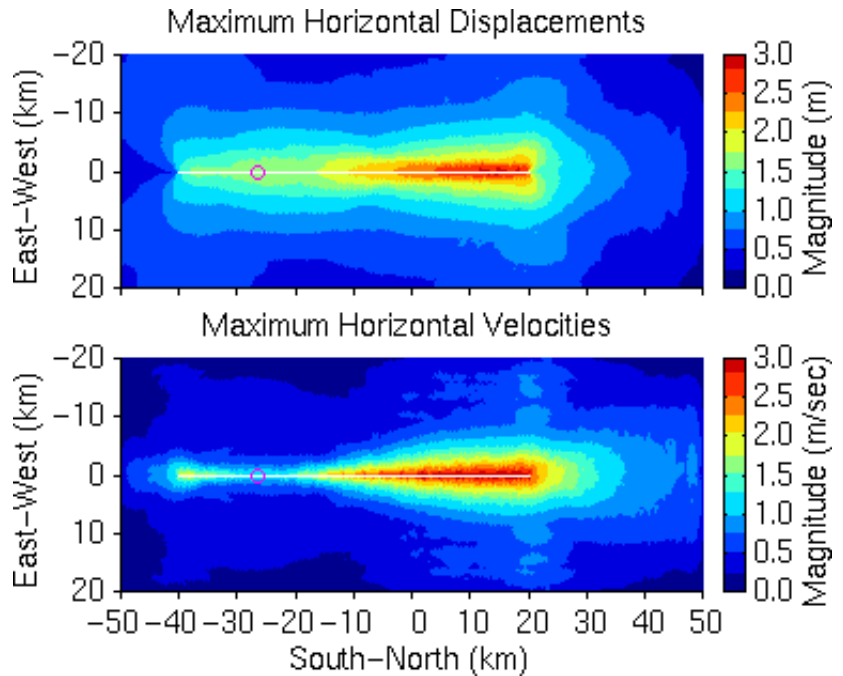


Figure 5: Maximum magnitudes of the horizontal displacement and velocity vectors at each point on the ground surface. The white line indicates the projection of the strike-slip fault onto the ground surface, and the purple circle identifies the epicenter.

peak to peak velocity. The directivity of the rupture causes large displacement and velocity pulses at site S1, while the velocity amplitudes at site S2 are about four times smaller. The acceleration response spectra in figure 6 reflect this disparity. The spectrum for site S1 lies between 0.6 g and 0.8 g for periods between 1.5 sec and 3.5 sec, while the entire spectrum for site S2 is below 0.2 g. Figure 7 shows the acceleration response spectra for periods of 2.0 sec, 3.0 sec, and 4.0 sec along the north-south line along the top of the fault and the east-west line across the north tip of the fault. The spectra along the north-south line increase along the strike of the fault away from the epicenter due to the directivity effect, and they decay rapidly at the ends of the fault. The response spectrum for a period of 2.0 sec exceeds 1.0 g along the northern half of the fault with a peak value of 1.4 g. The spectra along the east-west line decay rapidly with distance from the fault.

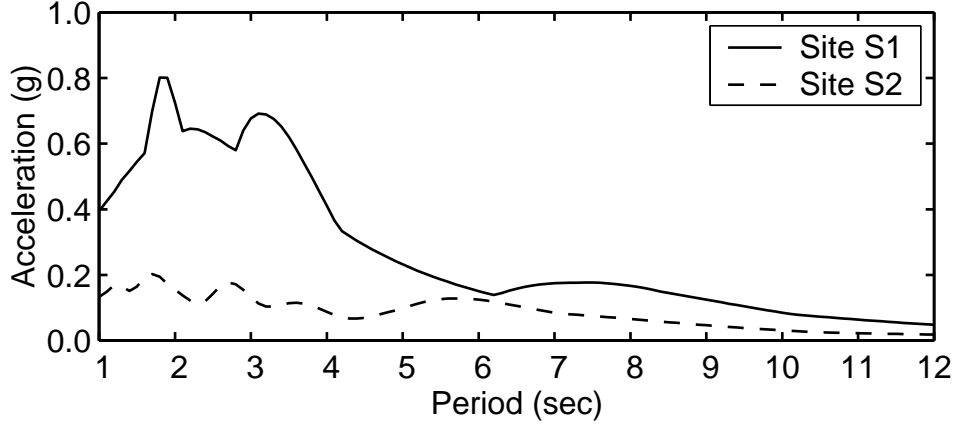


Figure 6: Horizontal acceleration response spectra at sites S1 and S2 for the strike-slip fault.

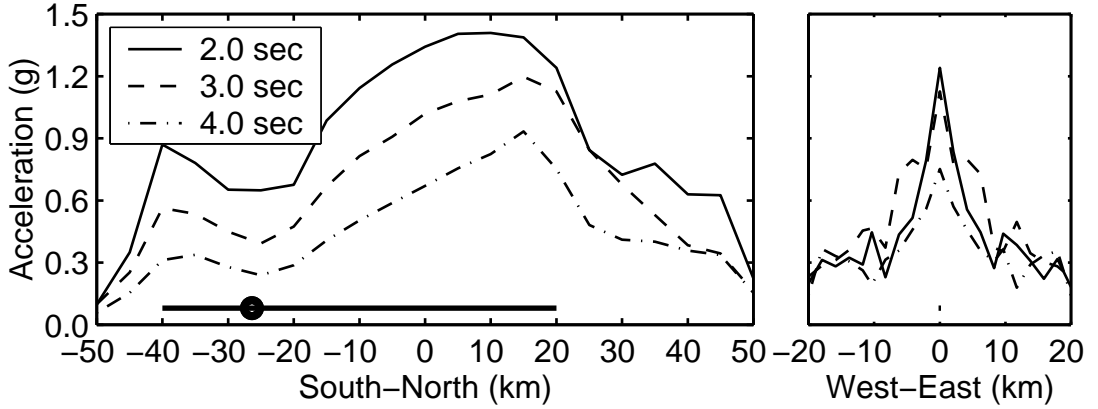


Figure 7: Horizontal acceleration response spectra for three periods along the north-south line running along the strike-slip fault (left) and along the east-west line running across the north tip of the fault (right). The thick lines at the bottom indicate the position of the fault surface and the dot identifies the epicenter.

Thrust Fault

The thrust fault closely resembles the Elysian Park fault underneath Los Angeles as described by Hall et al. (1995). We bury the 28 km long and 18 km wide fault 8.0 km below the ground surface. We impose shear tractions on the fault that dips 23 degrees to the north to generate oblique slip with a rake angle of 105 degrees from the strike to the west. We use the same depth variation of the material properties as in the strike-slip case. The finite-element model contains 5.1 million degrees of freedom and 7.7 million elements.

The rupture begins 4.0 km up-dip from the bottom of the fault along the fault centerline (location H in figure 8) and propagates at approximately 88% of the local shear wave speed in the direction of slip. The rupture produces an earthquake with an average slip of 1.6 m and a moment magnitude of 7.0. The 8.0 km depth of the top of the fault and the shallow dip cause the maximum horizontal displacements and velocities at the surface to occur 5.0 km up-dip from the top of the fault as shown in figure 9. A dependence of the rupture speed on the direction of propagation relative to the slip di-

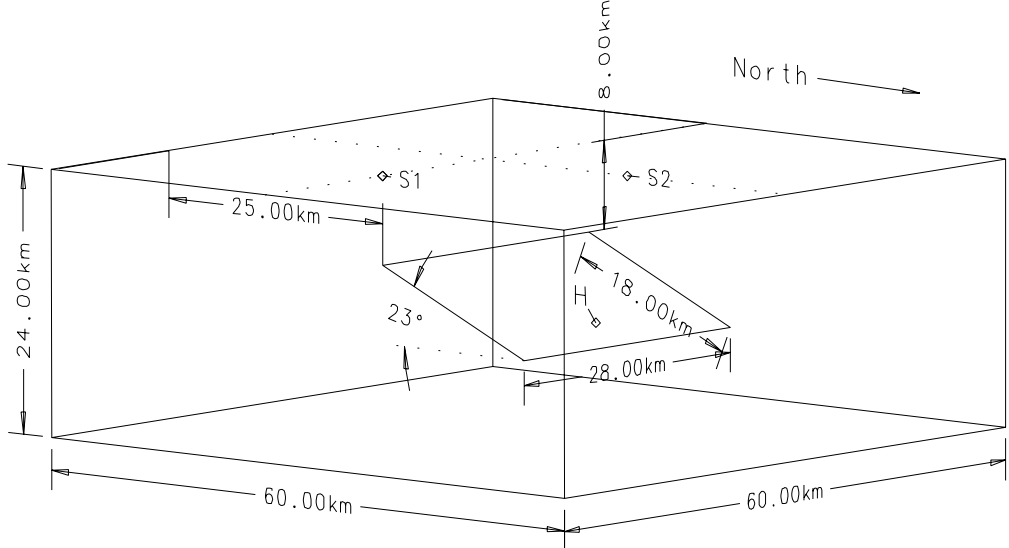


Figure 8: Domain geometry for the buried thrust fault.

rection (Madariaga et al. 1998; Aagaard 1999) causes large velocities above the lateral edges of the fault. On the ground surface the maximum velocities exceed 0.5 m/sec over an area of 830 square kilometers with a peak value of 1.1 m/sec. A large, single pulse in displacement and a corresponding large, double pulse in velocity dominate the ground motions in the forward direction. The ground motions toward the north (backward direction) do exceed 0.5 m/sec in some areas due to the bilateral nature of the latter portion of the rupture.

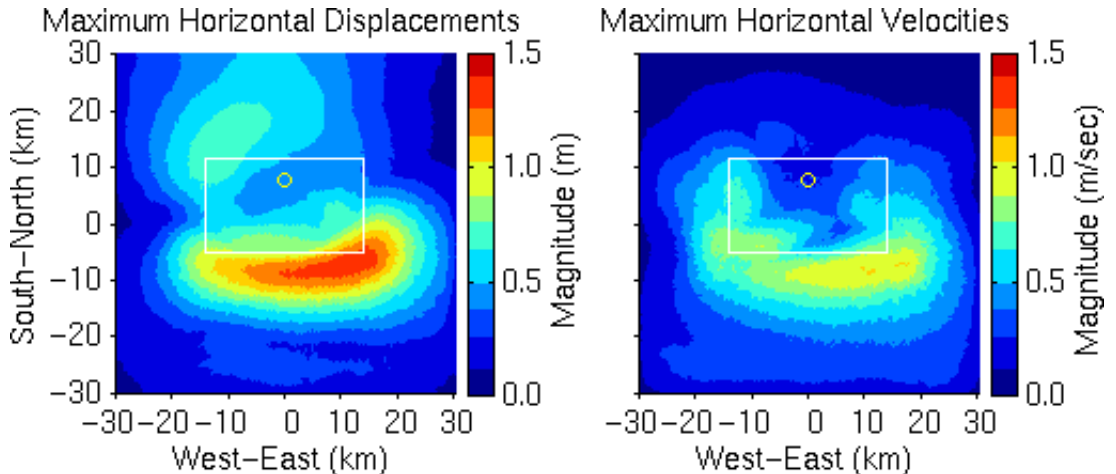


Figure 9: Maximum magnitudes of the horizontal and vertical displacement vectors at each point on the ground surface. The white line indicates the projection of the thrust fault onto the ground surface, and the yellow circle identifies the epicenter.

We compute the response spectra at sites S1 and S2 (see figure 8 for locations of the sites) following the same procedure that we used for the strike-slip fault. The horizontal acceleration response spectra shown in figure 10 illustrate the severity of the ground motion at site S1 compared to the ground motion at site S2. The spectrum for site S1 displays a broad peak of 0.45 g, while the spectrum for site S2 is relatively flat

with a level below 0.17 g. Figure 11 displays the acceleration response spectra for three periods along a north-south line over the center of the fault and along an east-west line above the top of the fault. As in the case of the strike-slip fault, in the north-south direction the spectra clearly show the effect of directivity with the largest values in the forward direction. The response spectrum for a period of 2.0 sec peaks at a value of 0.57 g at a location 4.2 km up-dip from the top of the fault. Along the east-west direction, the largest values occur above the top corners of the fault due to the bilateral nature of the latter portion of the rupture. The slip direction with a rake angle of 105 degrees causes slightly larger spectral values above the east corner compared to the west corner.

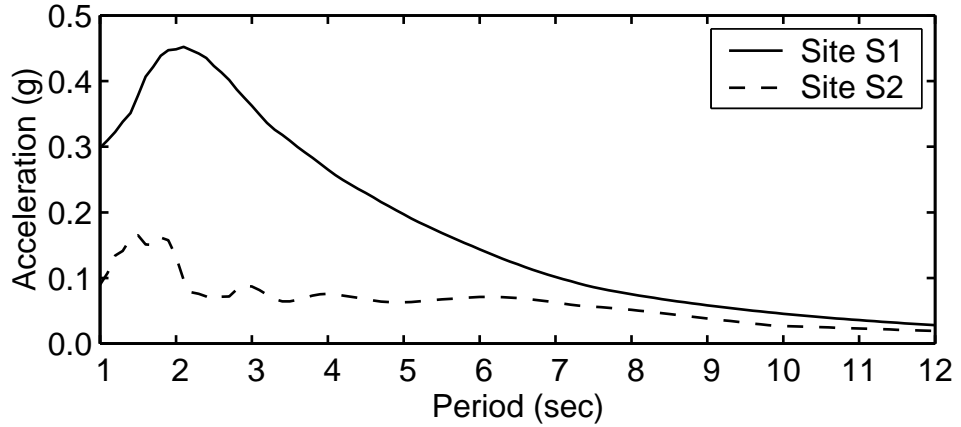


Figure 10: Horizontal acceleration response spectra at sites S1 and S2 for the thrust fault.

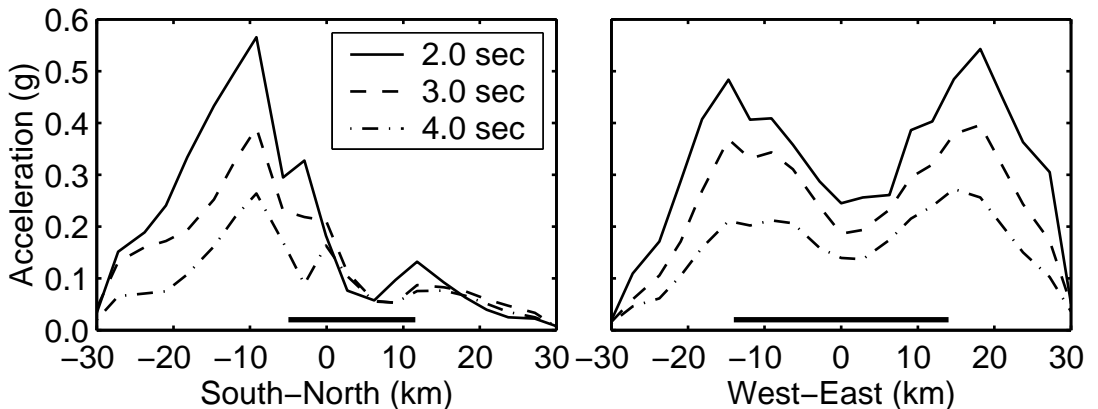


Figure 11: Horizontal acceleration response spectra for three periods along the north-south line running over the center of the thrust fault (left) and along the east-west line running over the top of the fault (right). The thick lines at the bottom indicate the position of the fault surface.

CONCLUSIONS

Dynamic rupture simulations can produce physically realistic ruptures and long-period earthquake ground motions. We need to know the initial conditions and the friction model, but not the complex relationships between the rupture speed, slip rate,

and final slip. On both the strike-slip fault and the thrust fault, the maximum displacements and velocities clearly show the effect of the directivity of the rupture. For the strike-slip fault the positive reinforcement of the shear wave by the rupture causes the displacements and velocities to increase along the fault away from the epicenter until the end of the fault where they decay rapidly with distance. The shape of the acceleration response spectra exhibits similar features. For the buried thrust fault the shallow dip of the fault causes the maximum displacements and velocities to occur up-dip from the top of the fault. The dependence of the rupture speed on the direction of propagation relative to the slip direction leads to the bilateral behavior of the latter portion of the rupture. This causes locally large velocities above the lateral edges of the fault. The large values in the response spectra at periods between 2.0 sec and 3.0 sec suggest that the near-source ground motions place large demands on structures with periods in this range. Because the large displacement and velocity pulses associated with the near-source ground motion occur across a broad range of scenarios (Aagaard 1999), we conclude that near-source ground motion poses a threat to long-period structures, especially those with periods in the range of a few seconds.

REFERENCES

- Aagaard, B. T. (1999). Finite-element simulations of earthquakes. Technical Report 99-03, California Institute of Technology, Earthquake Engineering Research Laboratory, Pasadena, CA.
- Bao, H. S., J. Bielak, O. Ghattas, L. F. Kallivokas, D. R. O'Hallaron, J. R. Shewchuk, and J. F. Xu (1998, January). Large-scale simulation of elastic wave propagation in heterogeneous media on parallel computers. *Computer Methods in Applied Mechanics and Engineering* 152(1-2), 85–102.
- Hall, J. F., T. H. Heaton, M. W. Halling, and D. J. Wald (1995, November). Near-source ground motion and its effects on flexible buildings. *Earthquake Spectra* 11(4), 569–605.
- Madariaga, R., K. Olsen, and R. Archuleta (1998, October). Modeling dynamic rupture in a 3D earthquake fault model. *Bulletin of the Seismological Society of America* 88(5), 1182–1197.
- Rao, S. S. (1999). *The finite element method in engineering* (3rd ed.). Boston: Butterworth Heinemann.